Adatom-induced variations of the atomic and electronic structures of Si(111)$\sqrt{3}\times\sqrt{3}$-Ag: A first-principles study

Hojin Jeong,[1] Han Woong Yeom,[1] and Sukmin Jeong[2,*]
[1]*Institute of Physics and Applied Physics and Center for Atomic Wires and Layers, Yonsei University, Seoul 120-746, Korea*
[2]*Department of Physics and Institute of Photonics and Information Technology, Chonbuk National University, Jeonju 561-756, Korea*
(Received 19 February 2008; revised manuscript received 20 May 2008; published 18 June 2008)

Using a first-principles calculation method, we study the changes in the atomic and electronic structures of the Si(111)$\sqrt{3}\times\sqrt{3}$-Ag surface (hereafter $\sqrt{3}$-Ag) via doping of extra Ag adatoms. We present a structural model for the adatom-induced $\sqrt{21}\times\sqrt{21}$ superstructure ($\sqrt{21}$-Ag), which has three Ag adatoms immersed into the substrate Ag layer within a unit cell. The present structural model reproduces well the measured scanning-tunneling-microscopy images as well as the electronic band structure measured by angle-resolved photoelectron spectroscopy. We find out that the complex band structure seen on the $\sqrt{21}$-Ag phase basically arises from the band folding of the original surface bands of $\sqrt{3}$-Ag. The extra Ag adatoms doped on $\sqrt{3}$-Ag modify only the band alignment without any additional adatom-induced surface state. The almost unoccupied two-dimensional free-electron-like band, generally called S_1, at pristine $\sqrt{3}$-Ag is gradually filled and shifted downward with an increase in the dopant coverage. As this shifted S_1 band crosses other surface bands, it loses its free-electron nature.

DOI: 10.1103/PhysRevB.77.235425 PACS number(s): 68.43.Fg, 68.43.Bc, 73.20.At

I. INTRODUCTION

The metallization of regularly ordered atomic overlayers or two-dimensional (2D) superstructures on semiconductor substrates is one of the most interesting subjects in surface science because they can serve for microscopic investigations of low-dimensional quantum phenomena such as quantum Hall effect,[1] quantum spin Hall effect,[2] and Rashba spin-orbit splitting.[3] Although 2D metallic superstructures are uncommon on semiconductor surfaces, a few metal/semiconductor heterostructures such as alkali-metal overlayers on Si(001) (Refs. 4 and 5) and Pb,[6] Au,[7] and Ag overlayers[8–32] on Si(111) can be metallized.

Among them, the Si(111)$\sqrt{3}\times\sqrt{3}$-Ag surface (hereafter referred to $\sqrt{3}$-Ag) has been studied most intensively mainly because of the systematic tunability of its metallic electron density by doping of extra metal adatoms.[8–13] The $\sqrt{3}$-Ag surface is formed on the Si(111) substrate by deposition of 1 monolayer (ML) Ag saturating all the dangling bonds of the surface Si atoms. Thus, the $\sqrt{3}$-Ag is nearly semiconducting originally with only a very small electron density at the Fermi level (E_F).[14–17] However, when a small amount (less than $\sim$0.1 ML) of monovalent metal adatoms such as noble and alkali metals are added on the pristine $\sqrt{3}$-Ag surface, an electron density at E_F gradually increases proportional to the adatom coverage.[8–13] That is, the pristine $\sqrt{3}$-Ag surface is metallized by the doping of extra adatoms. As the adatom coverage increases to 0.14–0.24 ML, a $\sqrt{21}\times\sqrt{21}$ superstructure ($\sqrt{21}$-Ag hereafter) commonly appears for any monovalent adsorbates.[12–14,18–28] A remarkably high electrical conductivity due to metallic surface bands has been reported on the $\sqrt{21}$-Ag surfaces formed with Au,[26] Ag,[27] and Na (Ref. 28) adatoms.

This interesting modification of the electronic structure of $\sqrt{3}$-Ag with the adatom doping is generally interpreted in terms of the electron transfer from the adatoms to the free-electron-like surface band.[8–13] However, the microscopic mechanism for the electronic-structure change in $\sqrt{3}$-Ag has not been made clear. Especially, the failure of the rigid-band model[10,11] and the splitting of the 2D free-electron-like band[11] observed on the $\sqrt{3}$-Ag surface cannot be explained by the simple charge transfer or doping model. In order to understand the microscopic mechanism, the structural information is essential. In this respect, the atomic structures of $\sqrt{3}$-Ag at low dopant coverages[29,30] are resolved in our previous theoretical study,[31] except for that of the $\sqrt{21}$-Ag phase appearing at a higher coverage. Though several structural models for $\sqrt{21}$-Ag have been proposed to date through scanning-tunneling microscopy (STM),[18–21] x-ray diffraction,[22] and reflection-high-energy-electron-diffraction methods,[23] even the optimum adatom coverage of this phase is still under debate. Figure 1shows four different structural models proposed previously, where three,[18,19] four,[20] and five[21] adatoms per $\sqrt{21}\times\sqrt{21}$ unit cell are suggested to sit *above* the substrate Ag layer.

In this paper, using a first-principles calculation method, we investigate the evolution of the electronic structures during the structural transformation from $\sqrt{3}$-Ag to $\sqrt{21}$-Ag. Since the monovalent adatoms on $\sqrt{3}$-Ag bring about basically the same structural and electronic properties,[8,12,13,19,24,28] we concentrate only on the case of the Ag adatom. For a systematic investigation, we extensively search for the atomic structure of $\sqrt{21}$-Ag at various Ag-adatom coverages and find out that the structure with *three-immersed* adatoms within a unit cell is energetically the most favorable. This structure reproduces well the measured STM images and the surface-band dispersions of $\sqrt{21}$-Ag. Based on the atomic structure of the present $\sqrt{21}$-Ag model and that at a lower adatom coverage in Ref. 31, we show how the electronic structure of the $\sqrt{3}$-Ag surface varies with the density of Ag adatoms and briefly discuss the origin of the variation.

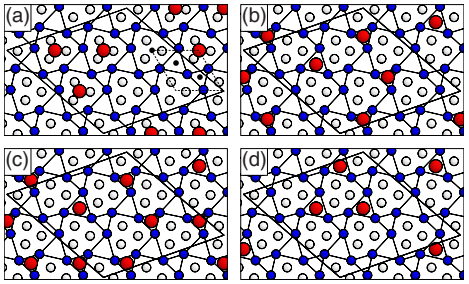

FIG. 1. (Color online) Schematics for the structural models of the $\sqrt{21}$-Ag phase proposed by (a) Ichimiya *et al.* (Ref. 18), (b) Tong *et al.* (Ref. 20), (c) Nogami *et al.* (Ref. 21), and (d) Liu *et al.* (Ref. 19). The white spheres represent the substrate Si atoms forming Si triangles and the (normal-sized) blue and (large) red spheres represent the substrate Ag and Ag adatoms, respectively. The rhombuses drawn by solid and dashed lines indicate the $\sqrt{21}\times\sqrt{21}$ and $\sqrt{3}\times\sqrt{3}$ unit cells, respectively. In (a), three natural adsorption sites for extra metal adatoms at the centers of Si triangle (SiT), small Ag triangle (ST), and large Ag triangles (LT) are marked by small circles.

II. CALCULATION METHOD

First-principles total-energy calculations are performed using the Vienna ab-initio simulation package (VASP) (Ref. 33) with ultrasoft pseudopotentials[34] and generalized-gradient approximation of Perdew and Wang[35] for the exchange-correlation energy. The surface is modeled by a repeated slab with a $\sqrt{21}\times\sqrt{21}$ periodicity, where a Ag layer, seven Si layers, and a H layer terminating the bottommost Si layer are included. Each slab is separated by an ~10-Å-wide vacuum space. The 13 Ry cutoff energy is used to expand the wave functions within the plane-wave basis. Four uniformly distributed k points including the Γ point are taken in the integration over a surface Brillouin zone (SBZ). The bottommost Si and H atoms are fixed at their ideal positions with the calculated lattice constant of bulk Si (5.46 Å) and the calculated bond length of Si-H (1.49 Å). The remaining Si and Ag atoms are fully relaxed until the residual force at each atom becomes less than 0.02 eV/Å. The simulated STM images are obtained by the isodensity of the local density of states based on the Tersoff-Hamann approximation.[36] In order to check the reliability of the present calculations, we perform convergence tests with increasing the cutoff energy and the number of k points. The results show that the adsorption energies of adatoms on the $\sqrt{21}\times\sqrt{21}$ supercell do not change within 0.02 eV when we increase the cutoff energy to 20 Ry and the number of k points to nine. This means that the present calculational parameters are sufficient for reliable results.

III. RESULTS AND DISCUSSION

A. Atomic structure

The previous studies for the extra adatoms on the $\sqrt{3}$-Ag surface reported that the $\sqrt{21}$-Ag structure is induced by monovalent adatoms of 0.14–0.24 ML without significantly destroying the underlying $\sqrt{3}\times\sqrt{3}$ framework.[18–23,27] Thus,

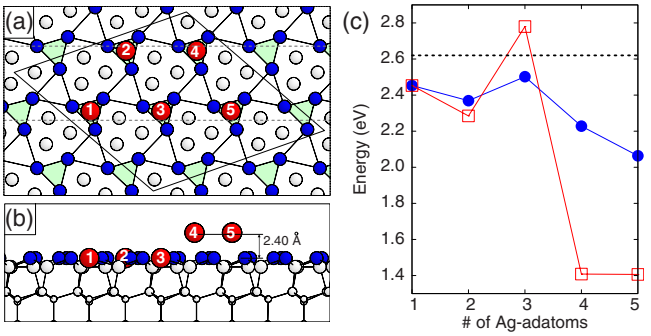

FIG. 2. (Color online) Schematics for (a) topview and (b) sideview of the most stable adsorption structures at the coverages from one to five Ag adatoms per $\sqrt{21}\times\sqrt{21}$ unit cell. In (b), only the atoms lying between two dashed lines drawn in (a) are shown. The small white spheres stand for the Si atoms in deep layers and the others are the same as in Fig. 1. (c) Adsorption energy (E_a, filled circles) and addition energy of the Ag adatom (E_{add}, open boxes) as a function of Ag-adatom coverage, defined as $E_a=[E(0)+NE_{\mathrm{Ag}}-E(N)]/N$ and $E_{\mathrm{add}}=E(N-1)+E_{\mathrm{Ag}}-E(N)$, respectively, where $E(N)$ and E_{Ag} represent the surface energy with N Ag adatoms and the atomic energy of a freestanding Ag atom in vacuum, respectively. The shaded triangles in (a) denote small Ag triangles in the pristine IET structure and the dotted line in (c) indicates the energy of bulk Ag of 2.62 eV/atom for reference.

the atomic structure of $\sqrt{3}$-Ag can be a starting point for the investigation of the $\sqrt{21}$-Ag superstructure. The structural model for the ground state of the $\sqrt{3}$-Ag surface, so called the inequivalent triangle (IET) model,[15–17] is displayed in Figs. 1 and 2. This IET structure has three (meta)stable adsorption sites for monovalent metal adatoms at the centers of a Si triangle (SiT), a small Ag triangle (ST), and a large Ag triangle (LT),[17,31] as marked in Fig. 1(a). In our previous study for low-coverage metal adatoms on the pristine IET structure, we showed that the metal adatoms (i) are the most stable at the ST site, (ii) spontaneously incorporate into the substrate Ag layer, and (iii) favor to form a cluster with adatoms immersed at three neighboring ST sites around a large Ag triangle.[31]

In order to determine the high-coverage adsorption structure of $\sqrt{21}$-Ag, we add Ag adatoms on $\sqrt{3}$-Ag from one (0.05 ML) to five adatoms (0.24 ML) in a $\sqrt{21}\times\sqrt{21}$ unit cell, where seven equivalent positions for each adsorption site (ST, LT, and SiT) exist. We initially put Ag adatoms on these positions with various adsorption configurations and then obtain the equilibrium structures by performing the structural relaxations. We check various inequivalent adsorption configurations over 30, but only the most stable adsorption configuration at each coverage is displayed schematically in Figs. 2(a) and 2(b).

As shown in Fig. 2, the adsorption behavior abruptly changes over the adatom coverage of 0.14 ML (three Ag adatoms per $\sqrt{21}\times\sqrt{21}$ unit cell). Up to 0.14 ML, the adsorption properties at lower coverages, summarized above, are basically preserved. The extra Ag adatoms energetically favor to sit on ST sites [see Fig. 2(a)] and are spontaneously *immersed* into the substrate Ag layer [see Fig. 2(b)]. The immersed adatoms reside at almost the same vertical posi-

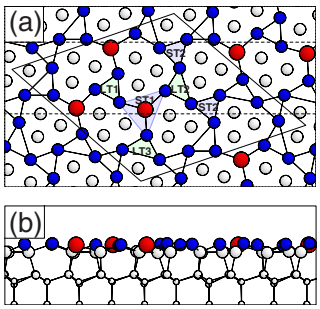

FIG. 3. (Color online) Fully optimized geometry of the present structural model for $\sqrt{21}-$Ag with three-immersed Ag adatoms: (a) Topview and (b) sideview, where only the atoms within two dashed lines in (a) are depicted. Five characteristic Ag triangles, which are drastically changed from the large (LT1–LT3) and the small (ST1–ST2) Ag triangles upon adsorption, are marked as shades in (a) for reference. The rhombus in (a) indicates the $\sqrt{21}\times\sqrt{21}$ unit cell. For symbols representing atoms, see Figs. 1 and 2.

tions as that of the substrate Ag layer. This is well consistent with our previous result[31] for the metal adatoms at low coverages, as described above, but in sharp contrast to the previously suggested models[18–23] with the adatoms above the substrate Ag layer. For one and two adatoms per unit cell, the adsorption energies are calculated as 2.45 and 2.37 eV/Ag, respectively, at any ST sites in a unit cell. At these coverages, the LT and SiT sites are less stable than the ST site by ~0.20 and ~1.30 eV, respectively, irrespective of the details of adsorption configurations. For three adatoms per unit cell, the adsorption energy is maximized as 2.50 eV/Ag when the adatoms are positioned at three neighboring ST sites around a large Ag triangle [see Fig. 2(a)], as being similar to the adatom cluster at lower coverages. Other arrangements with adatoms at ST sites, i.e., adatoms at three ST sites around a Si triangle, are less stable by ~0.10 eV. If the adatoms are immersed at three LT sites, the surface becomes less stable by ~0.10 eV.

On the other hand, beyond the critical coverage of 0.14 ML, the fourth and the fifth Ag adatoms sit on ST sites but significantly above the substrate Ag layer by ~2.40 Å. That is, the available space for the adatom immersion is fully saturated at the critical coverage of 0.14 ML, as will be discussed further below. We note that these high-coverage adsorptions do not destroy noticeably the prebuilt three-adatom-immersed structure, as schematically displayed in Figs. 2(a) and 2(b). The energy changes with the addition of a Ag adatom, i.e., the addition energies [open symbols in Fig. 2(c)], are only 1.40 eV for both the fourth and the fifth adatoms. Thus, the adsorption energies significantly decrease compared to that of the three-adatom-immersed structure by 0.27 and 0.44 eV/Ag at four and five adatoms, respectively [filled symbols in Fig. 2(c)].

Therefore, we suggest the three-adatom-immersed structure with the highest adsorption energy of 2.50 eV/Ag as the atomic structure of $\sqrt{21}$-Ag. The optimized geometry of the structure is displayed in Fig. 3. The local geometry around the adatoms is basically the same as that of the three-immersed-adatom cluster seen at low coverages [see Fig. 5(b) of Ref. 31]. This implies that the adatom cluster appearing at low coverages[29,30] is the basic building unit in forming the $\sqrt{21}$-Ag superstructure, as suggested by Liu *et al.*[19] The Si triangles are nearly unchanged upon adsorption (the side lengths of 2.52 vs 2.44–2.63 Å before and after the adsorption, respectively), while the Ag triangles undergo structural changes significantly due to the immersed adatoms. Two kinds of the Ag triangles in the pristine $\sqrt{3}$-Ag surface with side lengths of 3.00 and 3.88 Å are split into five characteristic triangles upon adsorption [LT1–LT3 and ST1–ST2 in Fig. 3(a)]. These are aligned with threefold rotational symmetry with respect to the center of the Ag triangle surrounded by three Ag adatoms (LT1). The area of the small triangle containing an adatom (ST1) is expanded greatly by ~160% (3.90 vs 10.13 Å^2 before and after the adsorption) with side lengths of 4.52–5.13 Å. The bond distances between the Ag adatom and the Ag atom at apexes of the triangle are calculated as ~2.85 Å. On the other hand, the unoccupied small Ag triangle (ST2) is contracted only by 3% with side lengths of 2.91–3.00 Å because it is rather far from the adatoms. The expansion of ST1 leads to the contraction of its three neighboring large Ag triangles (LT1–LT3). The area of the center large triangle surrounded by the Ag adatoms (LT1) is shrunken by 45% (6.52 vs 3.58 Å^2 before and after the adsorption) with equilateral side lengths of 2.87 Å. The contractions of the other two neighboring large triangles, LT2 and LT3, amount to 39% (3.99 Å^2) and 37% (4.13 Å^2) with their side lengths of 2.82–4.01 and 2.83–3.99 Å, respectively. As a result, the average distance between the Ag atoms (including the adatoms) is drastically reduced to 2.97 Å (from 3.44 Å of the pristine IET model) which is very close to the calculated interatomic distance of bulk Ag of 2.94 Å. This suggests that the Ag-Ag bond strength is optimized with three-immersed adatoms per $\sqrt{21}\times\sqrt{21}$ unit cell. Thus, the adatom immersion is saturated and the surface is stabilized at the coverage of 0.14 ML.

For comparison of the present structural model with the previously proposed ones shown in Fig. 1, we also position the Ag adatoms as in these models and perform structural relaxations. The results show that, except for the model by Ichimiya *et al.*[18] [Fig. 1(a)], three of the Ag adatoms are spontaneously incorporated into the substrate Ag layer, even though all of the adatoms are initially positioned at 2.40 Å above the substrate Ag overlayer. In the final structure based on the model by Liu *et al.*[19] [Fig. 1(d)], three Ag adatoms are immersed at LT sites. This structure is less stable than the present model only by ~0.10 eV. The final structures starting from the models by Tong *et al.*[20] and Nogami *et al.*[21] [Figs. 1(b) and 1(c), respectively] are highly unstable than the present model with the adsorption energies of 2.17 and 2.01 eV/Ag, respectively, due to the remaining adatoms above the Ag layer. On the other hand, in the optimized structure based on the model by Ichimiya *et al.*[18] [see Fig. 1(a)], the Ag adatoms at three SiT sites are positioned above 1.54 Å from the substrate Ag layer with an adsorption energy of 1.19 eV/Ag, significantly smaller (less favorable) than that of the present $\sqrt{21}$-Ag model by 1.31 eV/Ag.

The present results provide a natural explanation for the formation of the metastable $\sqrt{21}$-Ag superstructure; the $\sqrt{21}$-Ag phase is formed only below RT and, as the temperature increases, the phase changes to pristine $\sqrt{3}$-Ag. The im-

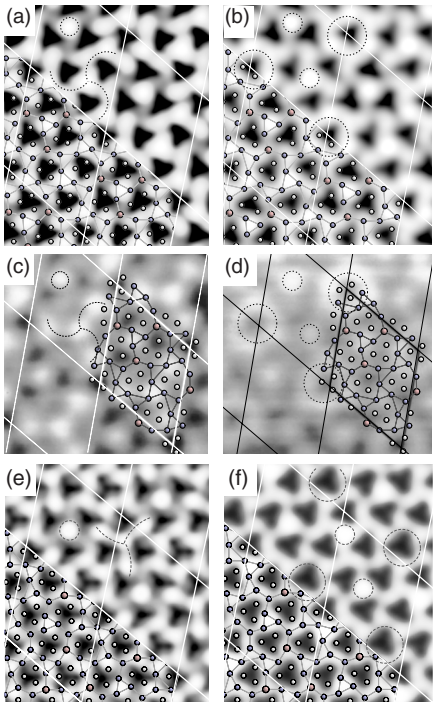

FIG. 4. (Color online) Simulated STM images for [(a) and (b)] the present structural model of $\sqrt{21}$-Ag with adatoms immersed at ST sites and for [(e) and (f)] the optimized Liu model with adatoms immersed at LT sites [see Fig. 1(d)]. All the simulated STM images are obtained with isosurfaces of electron density of 2.8 millielectron/Å^3. The average heights from the surfaces and the overall corrugations of the simulated STM images are [(a) and (e)] about 2.6 and 1.5 Å for the filled-state images and [(b) and (f)] about 2.8 and 1.4 Å for the empty-state images, respectively. [(c) and (d)] Experimental STM images taken from Figs. 8(b) and 8(e) of Ref. 12, respectively, where the present structural model for $\sqrt{21}$-Ag is superimposed. Biases for [(a), (c), and (e)] filled-state and [(b), (d), and (f)] empty-state images are −1 and +1 V, respectively. On all the images, the $\sqrt{21}\times\sqrt{21}$ periodic meshes (solid lines) and the key topographic patterns of the measured STM images (dashed circles and curves) are drawn. The contrasts of the simulated STM images are marginally modified.

mersed Ag adatoms at lower coverages than 0.14 ML are strongly confined within the 2D Ag overlayer without any metastable position above the Ag overlayer. Therefore, the nucleation of Ag adatoms into three-dimensional (3D) islands would be greatly suppressed, giving rise to the stability of $\sqrt{21}-$Ag. However, if the temperature increases, because the adsorption energy of the immersed adatom ($\leq$2.50 eV) is smaller than the energy of bulk Ag (2.62 eV), the Ag adatoms would prefer to nucleate over the potential barrier confining adatoms within the 2D surface layer. Thus, the surface would return to pristine $\sqrt{3}$-Ag with the formation of 3D Ag islands.[27]

B. Scanning-tunneling microscopy simulations

The comparison of simulated and experimental STM images strongly supports the present structural model for the $\sqrt{21}$-Ag surface. Figure 4shows simulated and measured STM images[12] with filled and empty biases of $\pm$1.0 V. The measured filled-state STM image [see Fig. 4(c)] is characterized by a propellerlike bright feature and a bright spot in a $\sqrt{21}\times\sqrt{21}$ unit cell. On the other hand, the empty-state image [Fig. 4(d)] exhibits ringlike patterns at the apexes of the unit cell and two bright spots within the boundary. The present structure reproduces not only these characteristic topographical patterns but also the alignments of the patterns at both filled and empty states [see Figs. 4(a) and 4(b)]. In the simulated STM image at the filled state [Fig. 4(a)], the Ag adatoms as well as Si triangles look dark, while the Ag triangles without a Ag adatom look bright. Thus, the center Ag triangle (LT1 in Fig. 3) surrounded by the Ag adatoms looks like a bright protrusion and the network of the unoccupied small Ag triangles (brighter: ST2 in Fig. 3) and shrunken large Ag triangles (less bright: LT2 and LT3 in Fig. 3) appears as a propeller. In the empty-state image of Fig. 4(b), unlike the filled-state image, the small triangles and the shrunken large triangles with medium brightness form the ringlike pattern at the apex of the boundary of the unit cell. Two bright protrusions with high brightness are due to the center Ag triangle (LT1) surrounded by the Ag adatoms and the unoccupied small Ag triangle (ST2).

Since the structures with immersed adatoms, but in different adsorption configurations from the present model, are energetically comparable with the present model within 0.1 eV, we check the STM images of those structures. Among them, the simulated STM images of the optimized Liu's model, for examples, are displayed in Figs. 4(e) and 4(f). As seen in the figures, the key topographical patterns of the measured STM images are also reproduced in the simulated STM images, but the alignments of these patterns match with the measured images only at the empty state [Fig. 4(f)]. In the filled-state image [Fig. 4(e)], the propellerlike patterns are largely rotated compared to the measured filled-state image. We note that other structures with immersed adatoms have similar discrepancy in their filled-state STM images (data not shown here). We also simulate the STM images of the previous structural models with adatoms above the Ag layer (the optimized structures from the models shown in Fig. 1, except for the Liu's model). However, all of these structures produce only bright protrusions at the adatom positions in the simulated STM images at both filled and empty states (results not shown here), in sharp contrast to the measured STM images showing the strong polarity dependence. These clear disagreements further support the present structural model with adatoms immersed at three neighboring ST sites in a unit cell.

C. Electronic structure

Next, we investigate the evolution of the electronic structure of $\sqrt{3}-$Ag via the doping of Ag adatoms. The calculated band structures for pristine $\sqrt{3}$-Ag and Ag-adatom-doped surfaces by one (0.05 ML) and three (0.14 ML) Ag adatoms per $\sqrt{21}\times\sqrt{21}$ unit cell are displayed in Fig. 5with the corresponding experimental results.

In the pristine IET structure for $\sqrt{3}$-Ag, we find four surface states as denoted by S_1-S_4 in Fig. 5(a). The nearly

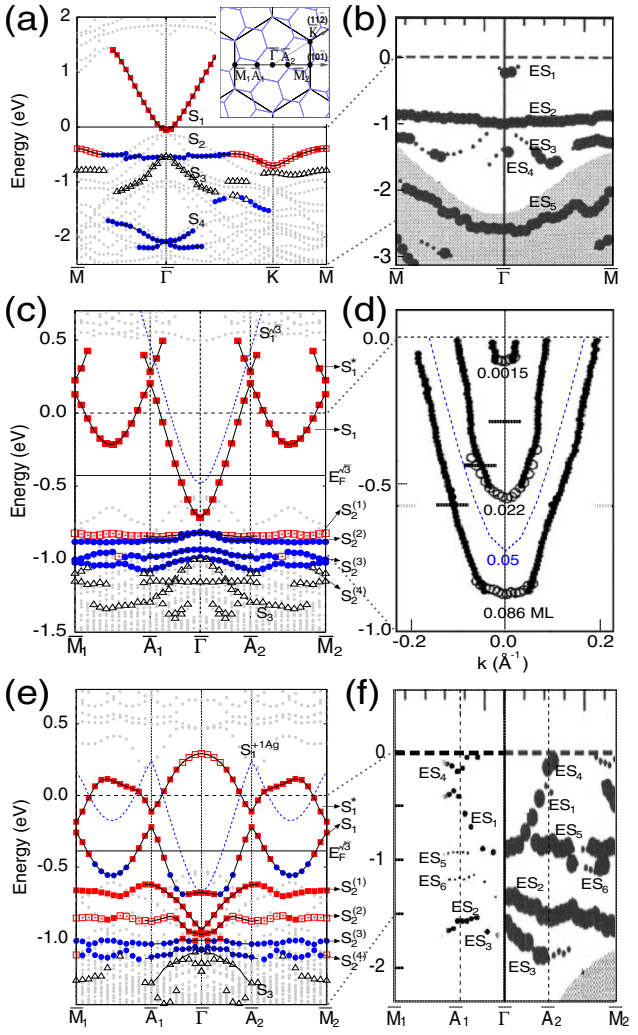

FIG. 5. (Color online) Calculated and measured band structures for [(a) and (b)] pristine $\sqrt{3}$-Ag, [(c) and (d)] Ag-adatom-doped $\sqrt{3}-$Ag, and [(e) and (f)] $\sqrt{21}$-Ag. The experimental data are taken from (b) Refs. 13, (d) 10, and (f) 13 and 14(for right and left panels with respect to $\bar{\Gamma}$), respectively. The inset in (a) shows the SBZ of the $\sqrt{3}$-Ag and $\sqrt{21}$-Ag surfaces. In the calculated band structures, the surface states mainly originating from Si and Ag atoms forming triangles are indicated by open and filled symbols representing the surface-parallel ($p_{\|}$, boxes), surface-perpendicular ($p_{\perp}$, upper-triangles), and spherical-symmetric (s, circles) orbital components, respectively. The gray dots indicate the bulk-Si states. In (c) and (e), the E_F of the pristine $\sqrt{3}$-Ag surface ($E_F^{\sqrt{3}}$) are marked by the horizontal solid lines, and the S_1 bands of the pristine $\sqrt{3}$-Ag($S_1^{\sqrt{3}}$) and 0.05 ML adatom-doped surface ($S_1^{+1\mathrm{Ag}}$) are marked by the dashed curves. In (d), short-thick lines indicate the positions of the measured VBM relative to E_F of the adatom-doped surfaces by 0.0015, 0.022, and 0.086 ML, from top to bottom. The calculated S_1 band at 0.05 ML is drawn by the dashed curve for reference. In all figures, the energy zero is E_F of the corresponding surfaces.

parabolic dispersive band, S_1, exhibits an isotropic dispersion along both the $\bar{\Gamma}$-$\bar{M}(10\bar{1})$ and the $\bar{\Gamma}$-$\bar{K}(11\bar{2})$ directions within the band gap of bulk Si, implying the 2D free-electron-like character as reported in the photoemission spectroscopy (PES) experiments.[8–13] This S_1 band mainly originates from the surface parallel ($p_{\|}$) components of Ag $5p$.[12,17] The bottom of the S_1 band is located just below 0.06 eV from the Fermi level at $\bar{\Gamma}$ and 0.08 eV higher than the valance-band maximum (VBM) (0.14 eV below the Fermi level at $\bar{\Gamma}$), respectively. That is, S_1 is almost unoccupied at the pristine $\sqrt{3}$-Ag surface. In contrast, the S_2 band is confined at a narrow energy range between −0.24 (at $\bar{M}$) and −0.57 eV (at $\bar{K}$) from the VBM with little dispersion. This band comes mainly from Si $3p_{\|}$ with a contribution of Ag $5p_{\|}$ near the SBZ boundary and from Ag $5s$ with a contribution of Si $3p_{\|}$ around the $\bar{\Gamma}$ point. This suggests that S_2 originates from the covalent interaction between Si and Ag. The other two surface bands, S_3 and S_4, are due to the backbonds of the topmost Si atoms forming Si triangles and the $5s$ component of surface Ag atoms, respectively. These surface bands match well with the measured band dispersions [Fig. 5(b)],[13] when the fully occupied S_2-S_4 bands are shifted downward by ~0.5 eV. The calculated S_1-S_3 and S_4 bands correspond to ES_1-ES_3 and ES_5 (or S_1-S_3 and S_5 in Ref. 13). These were shown to be mainly composed of $p_{\|}$-(ES_1), $p_{\perp}$-(ES_3), and s-orbital (ES_2 and ES_5) components,[12] in accord with the present results.[37] The effective mass of the S_1 band is calculated as $0.17m_e$, where m_e is the mass of a free electron. This also agrees relatively well with the experimental values of $(0.07-0.25)m_e$.[9,32]

One of the most interesting features in the electronic structure of the $\sqrt{3}$-Ag surface is the systematic variation of the occupation of S_1 by doping of a small amount of monovalent metal adatoms [see Fig. 5(d)]. This feature is commonly attributed to the electron donation from the adatoms to the S_1 band.[8–12] However, although the electron-doping scenario explains well the filling of the S_1 band, the details of the band modification are not consistent with the rigid-band model underlying this scenario. The rigid-band model says that the doping of electrons just pushes E_F upward without any change in the band structure itself. However, two recent experiments by Crain *et al.*[10] and Liu *et al.*[11] showed that the S_1 band splits with a gap opening by a small amount of adatoms at low temperatures. They argued that this subtle band splitting is due to the hybridization of the S_1 band with an impurity state formed by the adatoms. In addition, both experiments revealed that the S_1 band, although the other bands exhibit no energy shift, continuously shifts toward the higher binding energies, in clear contradiction to the simple rigid-band model [see Fig. 5(d)]. This implies extra interaction beyond the simple charge transfer.

The electronic-structure variation of $\sqrt{3}$-Ag via doping of a small amount of Ag adatoms is simulated with the adatom-doped surface by 0.05 ML (see Fig. 2 of Ref. 31for details of the atomic structure). Because the surface is modeled with the $\sqrt{21}\times\sqrt{21}$ supercell, extra surface states beyond the original surface bands of pristine $\sqrt{3}$-Ag emerge in the electronic structure of the surface, as displayed in Fig. 5(c). That is due to band-to-band interactions between the original bands and the backfolded bands of the $\sqrt{21}\times\sqrt{21}$ SBZ. The S_1 and S_2 bands of the pristine IET structure split into two (S_1 and S_1^*) and four ($S_2^{(1)}-S_2^{(4)}$) bands with almost the same orbital components as the original surface bands of the pristine $\sqrt{3}$-Ag surface, respectively. The E_F of the doped surface

shifts upward by 0.42 eV relative to that of the pristine $\sqrt{3}$-Ag (0.14 vs 0.56 eV from VBM before and after the adsorption), and the $S_2^{(1)}$–$S_2^{(4)}$ bands are located at nearly the same energy range (−0.25 and −0.50 eV from VBM) as that of the S_2 band in the pristine IET structure, in accord with the rigid-band model. However, in sharp contrast to the rigid-band model but in accord with previous experiments,[10,11] the S_1 band anomalously shifts downward by 0.23 eV [see $S_1^{\sqrt{3}}$ and S_1 in Fig. 5(c)]. As a consequence, the bottom of the S_1 band is located at 0.71 eV [(0.06+0.23+0.42) eV] below E_F, which is comparable with the experimental values of ~0.54 and ~0.88 eV at the dopings of 0.022 and 0.086 ML, respectively[10] [see Fig. 5(d)].

This unexpected energy shift of the S_1 band is also seen in the previous first-principles calculation by Aizawa and Tsukada,[17] with a Ag adatom above the Ag overlayer in a $\sqrt{3}\times\sqrt{3}$ unit cell (0.33 ML). In their model, unlike the immersed adatoms in the present case, the Ag adatoms rarely change the underlying $\sqrt{3}$-Ag structure. Thus, the structural change in the Ag layer due to the immersed adatoms cannot be the primary origin for the shift of the S_1 band. We attribute this downward shift of the S_1 band to the electrostatic attraction between delocalized electrons (S_1) and positively charged metal ions. The doping of extra Ag adatoms will increase the density of delocalized electrons as well as that of the metal ions through the electron donation from the adatoms to the S_1 band. Thus, such an attraction would increase with the doping level, inducing a higher binding-energy shift of the S_1 band. In addition, because the immersed adatom increases (reduces) the bond strengths (lengths) among Ag atoms, this energy shift tends to be enhanced as adatoms are incorporated into the substrate; the average distances between Ag atoms of $\sqrt{3}$-Ag reduce to 3.30 from 3.44 Å with 0.05 ML adatoms immersed into the substrate Ag layer.

However, contrary to the experimental observations by Crain *et al.*[10] and Liu *et al.*,[11] the S_1 band simply shifts without any change in its dispersion in the present calculation. Furthermore, there is no adatom-induced bound states crossing the S_1 band below E_F for the doped surfaces, unlike the argument of Liu *et al.*[11] These results suggest that other types of surface defects, rather than adatoms, are associated with the band splitting of the S_1 band. For example, a domain boundary between two degenerate IET structures could be one of such defects, which appears inevitably at low temperature, while disappears at high temperature due to the rapid thermal fluctuation between two IET domains.[15,16]

The surface structure with the $\sqrt{21}\times\sqrt{21}$ periodicity at 0.05 ML and the corresponding electronic structure [Fig. 5(c)] are rather artificial since the phase transition to $\sqrt{21}$-Ag occurs only at the coverages between 0.14 and 0.24 ML. Nevertheless, the features in the electronic structure for 0.05 ML with the $\sqrt{21}\times\sqrt{21}$ periodicity provide a basic concept for the changes in the band structure during the phase transformation to $\sqrt{21}$-Ag. As shown in Fig. 5(e), the calculated electronic structure of the present $\sqrt{21}$-Ag model with two more Ag adatoms per unit cell is somewhat similar to that of the surface with single immersed adatom within the unit cell [Fig. 5(c)]. These band structures have the same components of the surface bands: S_1^*, S_1, $S_2^{(1)-(4)}$, and S_3 at the energy range from −1.5 to 0.5 eV. This implies that the complex band structure seen in the $\sqrt{21}$-Ag phase [see Fig. 5(f)] basically originates from the folding of the surface bands of the pristine $\sqrt{3}$-Ag. The extra Ag adatoms modify these surface bands marginally, except for a larger shift of S_1.

As extra Ag adatoms donate their 5*s* electrons into the $\sqrt{21}\times\sqrt{21}$ unit cell, the partially occupied S_1 band of the single-adatom-immersed surface becomes fully occupied. The empty S_1^* band with a sharp dispersion becomes partially filled, implying the strong metallic character of the $\sqrt{21}$-Ag surface. The S_1 band simply shifts by −0.43 eV, except around the $\bar{\Gamma}$ point [see $S_1^{+1\mathrm{Ag}}$ and S_1 in Fig. 5(e)], resulting in the shift of the S_1 band toward a higher binding energy by 0.72 eV (0.29+0.43 eV) from that of the pristine $\sqrt{3}$-Ag surface. This shift makes the S_1 band to cross the nondispersive S_2 band of the pristine $\sqrt{3}$-Ag around the $\bar{\Gamma}$ point, resulting in a gap opening at the intersections between S_1 and $S_2^{(1-2)}$ and in the flattening of the S_1 band.

It is interesting that E_F of the $\sqrt{21}$-Ag surface becomes slightly lower by 0.04 eV than that of the 0.05 ML adatom-doped surface. This implies that the downward shift of the S_1 band overcompensates the upward shift of E_F due to the electron transfer from the adatoms to the surface band. The strong downward shift or the stabilization of S_1 can be ascribed to the drastic decrease (increase) in the bond distances (strengths) between the Ag atoms at the present $\sqrt{21}$-Ag structure; the average Ag-Ag distances are 3.44, 3.30, and 2.97 Å for the $\sqrt{3}$-Ag, 0.05 ML adatom-doped, and $\sqrt{21}$-Ag surfaces, respectively. In addition, since the structural changes in the Ag layer due to the adatom immersion alter the bonding environment of the surface Si and Ag atoms, the splitting of the corresponding Ag-Si bonding state ($S_2^{(1)-(4)}$) tends to be enhanced. The splittings between $S_2^{(1)}$ and $S_2^{(2)}$ and between $S_2^{(2)}$ and $S_2^{(3)}$, compared to those of 0.05 ML case, increase by ~0.2 and ~0.15 eV along the $\bar{M}_{1(2)}$-$\bar{A}_{1(2)}$ line, respectively, while the nearly degenerate $S_2^{(3)}$ and $S_2^{(4)}$ bands are almost unchanged.

The present calculation for the electronic structure of $\sqrt{21}$-Ag is in good agreement with the measured band dispersions by Zhang *et al.*[14] and Matsuda *et al.*,[13] which are shown in the left and right panels in Fig. 5(f), respectively. In both experiments, besides the original surface bands, three new surface bands, denoted as ES_4, ES_5, and ES_6 in Fig. 5(f), are detected on the $\sqrt{21}$-Ag surface. These are apparently consistent with S_1^*, $S_2^{(1)}$, and $S_2^{(2)}$ in the present calculation, respectively, with a uniform energy shift of ~0.4 eV. The two closely lying bands of $S_2^{(3)}$ and $S_2^{(4)}$ in the calculation seem to be detected as a single band of ES_2 in the experiments. The splitting of the S_1 band with the crossing of the localized surface band of S_2 is clearly seen in the experiment by Zhang *et al.*,[14] where the dispersive ES_1 band (corresponding to the S_1 band in the calculation) becomes nondispersive while ES_6 (corresponding to $S_2^{(2)}$) dips around the $\bar{\Gamma}$ point.

IV. CONCLUSION

The evolution of the atomic and electronic structures of the Si(111)$\sqrt{3}\times\sqrt{3}$-Ag surface by the doping of the monova-

lent Ag adatoms has been investigated using a first-principles total-energy calculation method. We have found out that the adsorption behavior of the Ag adatoms on the $\sqrt{3}$-Ag surface critically depends on the adatom coverage. At a lower coverage than 0.14 ML (three Ag adatoms per $\sqrt{21}\times\sqrt{21}$ unit cell), the Ag adatoms are immersed into the substrate Ag overlayer with relatively large adsorption energies of 2.37–2.50 eV/Ag. On the other hand, the excess adatoms beyond the critical coverage of 0.14 ML are weakly bound above the Ag overlayer with the adsorption energies of ~1.40 eV/Ag. From the comparison of adsorption energies at various adatom coverages, we have proposed the $\sqrt{21}$-Ag superstructure as the structure with three-immersed Ag adatom in the $\sqrt{21}\times\sqrt{21}$ unit cell. The excellent agreement between the simulated and the measured STM images at both filled and empty states strongly supports the present structural model.

The changes in the electronic structure during the phase transition from $\sqrt{3}$-Ag to $\sqrt{21}$-Ag have also been explored. The electronic structure of the pristine IET surface consists of the surface states mainly originating from the Ag-Ag bonds composed of surface parallel p_x and p_y orbitals (S_1), Ag-Si bonds (S_2), backbonds between the topmost and subsurface Si atoms (S_3), and Ag $5s$ orbital (S_4). The free-electron-like S_1 band continuously shifts toward higher binding energies as the adatom coverage increases. On the other hand, the other surface bands exhibit no significant energy shifts. As a consequence, the S_1 band approaches to the S_2 band with an energy shift of 0.23 eV at the intermediate coverage of 0.05 ML and finally crosses the S_2 band with an energy shift of 0.72 eV in the $\sqrt{21}$-Ag surface with 0.14 ML. The crossing of the S_1 and S_2 bands gives rise to a splitting of the S_1 band through a resonant interaction with the S_2 band. We attribute the unusual energy shift of the S_1 band to the electrostatic attraction between delocalized S_1 electrons and positively charged Ag (ad)atoms. In addition, the folded bands due to the change in the surface periodicity emerge at the doped surfaces with both 0.05 and 0.14 ML coverages, which have the same origins in spite of different doping levels. Therefore, the electronic structure changes from $\sqrt{3}$-Ag to $\sqrt{21}$-Ag are the combined results of the downward shift of the S_1 band and the folding of the pristine surface bands into a reduced surface Brillouin zone of the $\sqrt{21}\times\sqrt{21}$ unit cell.

ACKNOWLEDGMENTS

This work was supported by the Korea Research Foundation Grant funded by the Korea Government (MOEHRD) (Grant No. KRF-2006-005-J00301) and Center for Atomic Wires and Layers of the CRI program by MOST of Korea.

*jsm@chonbuk.ac.kr

[1] K. Eng, R. N. McFarland, and B. E. Kane, Phys. Rev. Lett. **99**, 016801 (2007).
[2] C. L. Kane and E. J. Mele, Phys. Rev. Lett. **95**, 226801 (2005).
[3] J. Premper, M. Trautmann, J. Henk, and P. Bruno, Phys. Rev. B **76**, 073310 (2007).
[4] L. S. O. Johansson and B. Reihl, Phys. Rev. Lett. **67**, 2191 (1991).
[5] L. S. O. Johansson, T. Dütemeyer, L. Duda, and B. Reihl, Phys. Rev. B **58**, 5001 (1998).
[6] W. H. Choi, H. Koh, E. Rotenberg, and H. W. Yeom, Phys. Rev. B **75**, 075329 (2007).
[7] K. N. Altmann, J. N. Crain, A. Kirakosian, J. L. Lin, D. Y. Petrovykh, F. J. Himpsel, and R. Losio, Phys. Rev. B **64**, 035406 (2001).
[8] S. Hasegawa, X. Tong, S. Takeda, N. Sato, and T. Nagao, Prog. Surf. Sci. **60**, 89 (1999).
[9] J. N. Crain, K. N. Altmann, C. Bromberger, and F. J. Himpsel, Phys. Rev. B **66**, 205302 (2002).
[10] J. N. Crain, M. C. Gallagher, J. L. McChesney, M. Bissen, and F. J. Himpsel, Phys. Rev. B **72**, 045312 (2005).
[11] C. Liu, I. Matsuda, R. Hobara, and S. Hasegawa, Phys. Rev. Lett. **96**, 036803 (2006).
[12] X. Tong, S. Ohuchi, N. Sato, T. Tanikawa, T. Nagao, I. Matsuda, Y. Aoyagi, and S. Hasegawa, Phys. Rev. B **64**, 205316 (2001).
[13] I. Matsuda, T. Hirahara, M. Konishi, C. Liu, H. Morikawa, M. D'angelo, S. Hasegawa, T. Okuda, and T. Kinoshita, Phys. Rev. B **71**, 235315 (2005).
[14] H. M. Zhang, K. Sakamoto, and R. I. G. Uhrberg, Phys. Rev. B **64**, 245421 (2001).
[15] N. Sasaki, S. Watanabe, and M. Tsukada, Phys. Rev. Lett. **88**, 046106 (2002).
[16] K. Sakamoto, T. Suzuki, K. Mawatari, K. Kobayashi, J. Okabayashi, K. Ono, N. Ueno, and M. Oshima, Phys. Rev. B **73**, 193303 (2006).
[17] H. Aizawa and M. Tsukada, Phys. Rev. B **59**, 10923 (1999).
[18] A. Ichimiya, H. Nomura, Y. Horio, T. Sato, T. Sueyoshi, and M. Iwatsuki, Surf. Rev. Lett. **1**, 1 (1994).
[19] C. Liu, I. Matsuda, M. D'angelo, S. Hasegawa, J. Okabayashi, S. Toyoda, and M. Oshima, Phys. Rev. B **74**, 235420 (2006).
[20] X. Tong, Y. Sugiura, T. Nagao, M. Takami, S. Takeda, S. Ino, and S. Hasegawa, Surf. Sci. **408**, 146 (1998).
[21] J. Nogami, K. J. Wan, and X. F. Lin, Surf. Sci. **306**, 81 (1994).
[22] H. Tajiri, K. Sumitani, W. Yashiro, S. Nakatani, T. Takahashi, K. Akimoto, H. Sugiyama, X. Zhang, and H. Kawata, Surf. Sci. **493**, 214 (2001).
[23] Y. Fukaya, A. Kawasuso, and A. Ichimiya, Surf. Sci. **600**, 3141 (2006).
[24] M. D'angelo, M. Konishi, I. Matsuda, C. Liu, S. Hasegawa, T. Okuda, and T. Kinoshita, Surf. Sci. **590**, 162 (2005).
[25] H. M. Zhang, K. Sakamoto, and R. I. G. Uhrberg, Phys. Rev. B **70**, 245301 (2004).
[26] C.-S. Jiang, X. Tong, S. Hasegawa, and S. Ino, Surf. Sci. **376**, 69 (1997).
[27] X. Tong, S. Hasegawa, and S. Ino, Phys. Rev. B **55**, 1310 (1997).
[28] M. Konishi, I. Matsuda, C. Liu, H. Morikawa, S. Hasegawa, T. Okuda, and T. Kinoshita, e-J. Surf. Sci. Nanotechnol. **3**, 107 (2005).
[29] N. Sato, T. Nagao, and S. Hasegawa, Phys. Rev. B **60**, 16083

(1999).
[30] M. Ono, Y. Nishigata, T. Nishio, T. Eguchi, and Y. Hasegawa, Phys. Rev. Lett. **96**, 016801 (2006).
[31] H. Jeong, H. W. Yeom, and S. Jeong, Phys. Rev. B **76**, 085423 (2007).
[32] T. Hirahara, I. Matsuda, M. Ueno, and S. Hasegawa, Surf. Sci. **563**, 191 (2004).
[33] G. Kresse and J. Hafner, Phys. Rev. B **47**, 558 (1993); G. Kresse and J. Furthmüller, *ibid.* **54**, 11169 (1996).
[34] D. Vanderbilt, Phys. Rev. B **41**, 7892 (1990).
[35] J. P. Perdew and Y. Wang, Phys. Rev. B **45**, 13244 (1992).
[36] J. Tersoff and D. R. Hamann, Phys. Rev. Lett. **50**, 1998 (1983).
[37] The only one discrepancy between the theory and experiment is the existence of ES_4 only at the experiment. We think that this ES_4 band might be a resonance state of bulk band, rather than surface band, trapped in the forbidden region of Si(111)1×1.